Contribution of Coulomb Interactions to a Two-Step Crystal Structure Phase Transformation Coupled with a Significant Change in Spin Crossover Behavior for a Series of Charged Fe-…

Takahashi, Kazuyuki ; Okai, Mitsunobu ; Mochida, Tomoyuki ; Sakurai, Takahiro ; Ohta, Hitoshi ; Yamamoto, Takashi ; Einaga, Yasuaki ;…

(Citation)
Inorganic Chemistry,57(3):1277-1287

(Issue Date)
2018-02-05

(Resource Type)
journal article

(Version)
Accepted Manuscript

A Contribution of Coulomb Interactions to Two-step Crystal Structural Phase Transformation Coupled to the Significant Change in Spin Crossover Behavior for a Series of Charged Fe^{II} Complexes from 2,6-bis(2-methylthiazol-4-yl)pyridine

Kazuyuki Takahashi,[†,*] *Mitsunobu Okai,*[†] *Tomoyuki Mochida,*[†] *Takahiro Sakurai,*[‡] *Hitoshi Ohta,*[§] *Takashi Yamamoto,*[¶] *Yasuaki Einaga*,[¶] *Yoshihito Shiota*,[⊥] *Kazunari Yoshizawa*,[⊥] *Hisashi Konaka*,[#] and Akito Sasaki[#]

[†]Department of Chemistry, Graduate School of Science, Kobe University, 1-1 Rokkodai, Nada-ku, Kobe, Hyogo 657-8501, Japan; E-Mail: ktaka@crystal.kobe-u.ac.jp

[‡]Research Facility Center for Science and Technology, Kobe University, 1-1 Rokkodai, Nada-ku, Kobe, Hyogo 657-8501, Japan

[§]Molecular Photoscience Research Center, Kobe University, 1-1 Rokkodai, Nada-ku, Kobe, Hyogo 657-8501, Japan

[¶]Department of Chemistry, Faculty of Science and Technology, Keio University, 3-14-1 Hiyoshi, Kohoku-ku, Yokohama, Kanagawa 223-8522, Japan

[⊥]Institute for Materials Chemistry and Engineering, Kyushu University, 744 Motooka, Nishi-ku, Fukuoka 819-0395, Japan

[#]XRD Application & Software Development, Rigaku Corporation, 3-9-12 Matsubara-cho, Akishima, Tokyo 196-8666, Japan

ABSTRACT

A series of $[Fe^{II}(\mathbf{L})_2](BF_4)_2$ compounds were structurally and physically characterized (**L** = 2,6-bis(2-methylthiazol-4-yl)pyridine). The crystal structural phase transformation from dihydrate compound **1** to anhydrous compound **3** through partly hydrated compounds **2** and **2'** upon dehydration was found. The compounds **1** and **3** exhibited a gradual spin crossover (SCO) conversion, whereas the compounds **2** and **2'** demonstrated a two-step and one-step abrupt SCO transition, respectively. The X-ray single crystal structural analysis revealed that one-dimensional and two-dimensional Fe cation networks linked by π-stacking and sulfur-sulfur interactions were formed in **1** and **3**, respectively. The thermodynamic analysis of the magnetic susceptibility for **1**, **2'**, and **3** suggests that the enthalpy differences may govern SCO transition behaviors in the polymorphic compounds **2'** and **3**. The structural comparison between **1** and **3** indicates that the SCO behavior variations and crystal structural transformation in the present $[Fe^{II}(\mathbf{L})_2](BF_4)_2$ compounds can be interpreted by the relationship between the lattice enthalpies mainly arising from Coulomb interactions between the Fe cations and BF_4 anions like typical ionic crystals.

Introduction

An octahedral six-coordinate transition metal complex with d^4-d^7 electrons provides either a spin-parallel or spin-paired electronic configuration. The former refers to a high-spin (HS) state, the latter refers to a low-spin (LS) state. The change between the HS and LS states induced by temperature, pressure, and light, is called spin crossover (SCO), which represents one of the examples for molecular bistability. [1–3] Since an SCO conversion induces the change not only in spin multiplicity but also in color for a transition metal complex, SCO complexes have attracted a growing attention toward the development of magnetic memory, display, and sensing devices as potential future applications.[4]

The thermal behavior of an SCO complex in a solid state is classified into typical types, namely a Boltzmann-like equilibrium, gradual conversion, abrupt transition with or without a thermal hysteresis loop, and two-step transition.[3] These SCO behaviors represent the relationship of the spin-states between neighboring SCO complex molecules in a crystal. Among them the abrupt-type transition is the most intriguing from a point of view of the SCO cooperativity. The emergence of cooperativity is considered to be important to utilize an SCO compound as a molecular switching material.

One possible way to develop a new SCO compound exhibiting a cooperative SCO transition is the introduction of intermolecular interactions into the SCO compound. Numerous SCO compounds showing cooperative SCO transitions arising from intermolecular interactions such as π-stacking,[5–13] coordination-bonding,[14–22] hydrogen-bonding,[23–27] halogen-bonding,[28,29] and sulfur-sulfur interactions[30] have been reported to date. Although the cooperativity in these

SCO compounds is attributed to such intermolecular short contacts in most cases, it is very difficult to elucidate the role of intermolecular interactions for the SCO cooperativity.

An SCO phenomenon is known to be driven by the entropy difference (ΔS) between the LS and HS states arising from the change in spin multiplicity, and intra- and intermolecular vibrations.[31] On the other hand, the cooperativity in SCO originates from long-range elastic interactions based on electron-phonon coupling between SCO complex molecules.[32] Broadly speaking two types of thermodynamic models accounting for the cooperativity in SCO have been known to date.[33] One is the regular solution model[34] and the other is the domain model.[35] Since a thermal hysteresis effect can be described by the former and its modifications,[7,18,36,37] they have been widely applied to extract thermodynamic parameters of SCO transitions. In the regular solution model, interaction energy (Γ) is introduced to describe the SCO cooperativity. An abrupt SCO transition appears if the complex fulfills the condition of $\Gamma > 2RT_{1/2}$, where R is the gas constant and $T_{1/2}$ (= $\Delta H/\Delta S$) is an SCO transition temperature (ΔH is the enthalpy difference). Since polymorphs in SCO complexes give similar contributions to ΔS, they can be good candidates for elucidation of the role of intermolecular interactions in SCO behaviors from the relationship between Γ and ΔH. However, the correlation between intermolecular interactions and magnetic property in SCO polymorphs has been reported scarcely.

Recently we reported the SCO hybrid paramagnet, $[Fe^{II}(\mathbf{L})_2][Ni(dmit)_2]_2$ (**L** = 2,6-bis(2-methylthiazol-4-yl)pyridine, dmit = 4,5-dithiolato-1,3-dithiole-2-thione), which exhibited a complete gradual SCO conversion between $S = 0$ and $S = 2$ having a stable paramagnetic π-radical with $S = 1/2$ due to strong cation-anion interactions.[38] Despite the existence of strong π-stacking and chalcogen-bonding interactions, the SCO behavior of this complex was gradual. To

gain an insight into the correlation between intermolecular interactions and the SCO cooperativity, we were interested in the crystal structure of the parent $[Fe^{II}(\mathbf{L})_2]$ compound. Although Baker and Goodwin previously reported the synthesis, magnetic susceptibility, and Mössbauer spectroscopy of the parent compound $[Fe^{II}(\mathbf{L})_2](BF_4)_2$,[39] its crystal structure is still unknown. Hence we reinvestigated the preparation and crystal structural analysis of single crystals for $[Fe^{II}(\mathbf{L})_2](BF_4)_2$. As we tried to prepare single crystals from the parent compound, we found hydrate and anhydrous compounds having three structural phases, namely, dihydrate compound $[Fe^{II}(\mathbf{L})_2](BF_4)_2{\cdot}2H_2O$ (**1**), partly hydrated compound $[Fe^{II}(\mathbf{L})_2](BF_4)_2{\cdot}nH_2O$ (**2**: n = 1.4; **2'**: n ~ 0), and anhydrous compound $[Fe^{II}(\mathbf{L})_2](BF_4)_2$ (**3**) (Chart 1). Moreover, we discovered the crystal structural phase transformation from **1** to **3** through **2** and **2'**, which accompanied the significant change in SCO transition behavior. In addition, we also found the notable difference in the relaxation temperature from the photo-induced HS state between **2'** and **3**. The thermodynamic analysis for magnetic susceptibility indicates that the enthalpy differences may govern their SCO transition behaviors in the transformable polymorphs **2'** and **3**. Moreover, the comparison of the thermal variations in the crystal structures **1** and **3** implies that the Coulomb interactions between the Fe cation and BF_4 anion may play a central role in the SCO behaviors and crystal phase transformation in the charged $[Fe^{II}(\mathbf{L})_2](BF_4)_2$ compounds. We report herein the preparation, crystal structures, thermal, magnetic, and optical properties for the charged $[Fe^{II}(\mathbf{L})_2](BF_4)_2$ compounds.

Experimental Section

Preparation of the Fe(II) Complexes

All reagents were obtained from commercial sources and were used without further purification. Ligand **L** and the parent compound $[Fe(\mathbf{L})_2](BF_4)_2$ were prepared according to the literature.[38]

$[Fe(\mathbf{L})_2](BF_4)_2 \cdot 2H_2O$ (**1**). Recrystallization from an aqueous solution of $[Fe(\mathbf{L})_2](BF_4)_2$ gave dihydrate compound **1** as yellow needles. Anal. Calcd. for $C_{26}H_{26}N_6O_2B_2F_8FeS_4$: C, 38.45; H, 3.23; N, 10.35%. Found: C, 38.57; H, 3.21; N, 10.22%.

$[Fe(\mathbf{L})_2](BF_4)_2 \cdot n H_2O$ (**2**: $n = 1.4$; **2'**: $n \sim 0$). The dihydrate compound **1** was heated to 120 ˚C and then cooled to room temperature, affording partly hydrated compound **2** as a yellow powder. Anal. Calcd. for $C_{26}H_{24.8}O_{1.4}N_6B_2F_8S_4Fe$ ($n = 1.4$): C, 38.97; H, 3.12; N, 10.49%. Found: C, 38.98; H, 3.15; N, 10.38%. The compound **2'** was obtained by repeating the magnetic susceptibility measurements of either compound **1** or **2** in the MPMS chamber until the appearance of a one-step SCO transition.

$[Fe(\mathbf{L})_2](BF_4)_2$ (**3**). Recrystallization from an ethanol solution of $[Fe(\mathbf{L})_2](BF_4)_2$ gave anhydrous compound **3** as dark red platelets. Anal. Calcd. for $C_{26}H_{22}N_6B_2F_8FeS_4$: C, 40.23; H, 2.86; N, 10.83%. Found: C, 40.17; H, 2.88; N, 10.75%.

Physical Measurements

Variable temperature direct current magnetic susceptibilities of polycrystalline samples (ca. 20 mg) fold in a sealed gelatin capsule wrapping an aluminum foil or in an aluminum capsule with pinhole were measured on a Quantum Design MPMS-XL magnetometer under a field of 0.5 T in the temperature range of 2−300 K for **1**, **2**, and **2'** or 2−400 K for **3**. The sample magnetization data were obtained by the subtraction of background magnetization data from the measured data, and then the magnetic susceptibilities were corrected for diamagnetic contributions estimated by

Pascal constants.[40] The SCO transition temperature $T_{1/2}$ was defined by the center temperature between the minimum and maximum temperatures in the first order differential curves of the $\chi_M T$ products. The photo effect on the magnetization of a sample was examined by using a YAG laser (532 nm, CrystaLaser GCL-100L). The light was guided by a quartz optical fiber into the sample chamber of the magnetometer. The sample was placed between quartz rods and the upper rod was connected with one end of the optical fiber. The Mössbauer spectra for the powdered samples were recorded on a constant acceleration spectrometer with a source of ^{57}Co/Rh in the transmission mode. The measurements at low temperature were performed with a closed-cycle helium refrigerator (Iwatani Co., Ltd.). Velocity was calibrated by using an α-Fe standard at 293 K. The obtained Mössbauer spectra were fitted with asymmetric Lorentzian doublets by the least squares fitting program (MossWinn). The powder X-ray diffraction (XRD) profiles were obtained using a diffractometer (SmartLab, Rigaku) with monochromated Cu-$K\alpha$ radiation. The sample powders were placed on a glass holder. To determine the crystal structure of **2**, the sample powder was contained in glass capillaries (0.5 mm diameter) and sealed. Cu $K\alpha_1$ radiation monochromatized with a Ge(111) Johansson-type crystal monochromator was employed in the transmission method. The powder diffraction data were collected between 3 and 90 º at 2θ with a 0.005 step. The obtained diffraction peaks were indexed by using the program N-TREOR. All analyses were performed using integrated X-ray powder diffraction software (PDXL Version 2.1.1.4, Rigaku). The TG-DTA was performed using a Rigaku TG8120 analyzer at a scan speed of 2 K mol^{-1}.

Crystal Structure Determinations

A crystal was mounted in a polyimide loop or glass rod. A Nihon Thermal Engineering nitrogen gas flow temperature controller was used for the temperature variable measurements. All data were collected on a Bruker APEX II CCD area detector with monochromated Mo-$K\alpha$ radiation generated by a Bruker Turbo X-ray Source coupled with Helios multilayer optics. All data collections and calculations were performed using the APEX2 crystallographic software package (Bruker AXS). The data were collected to a maximum 2θ value of 55.0 º. A total of 720 oscillation images were collected. The APEX II program was used to determine the unit cell parameters and for data collection. Data were integrated by using SAINT. Numerical absorption correction was applied by using SADABS. The structures at all temperatures were solved by direct methods and refined by full-matrix least-squares methods based on F^2 by using the SHELXL program. All non-hydrogen atoms were refined anisotropically. Hydrogen atoms were generated by calculation and refined using the riding model. CCDC 1430814-1430817, 1581526-1581527 contain the supplementary crystallographic data for this paper. These data can be obtained free of charge via http://www.ccdc.cam.ac.uk/conts/retrieving.html (or from the CCDC, 12 Union Road, Cambridge CB2 1EZ, UK; Fax: +44 1223 336033; E-mail: deposit@ccdc.cam.ac.uk).

Results

Synthesis

The parent compound $[Fe(\mathbf{L})_2](BF_4)_2$ was prepared according to the literature.[38] Recrystallization from ethanol afforded anhydrous compound **3** as dark red platelets, whereas recrystallization from water gave dihydrate compound **1** as yellow needles. The compositions of **1** and **3** were determined by microanalysis and crystal structural analyses described below. Partly hydrated

compound **2** was unexpectedly obtained by heating the dihydrate compound **1** to 120 ˚C followed by cooling it to room temperature. The composition of **2** was confirmed by microanalysis and thermogravimetry.

Crystal Structural Transformation from 1 to 3

To investigate the thermal stability of the dihydrate compound **1**, the thermogravimetry differential thermal analysis (TG-DTA) for **1** was performed using a Rigaku TG8120 analyzer. The TG curves are shown in Figure 1. On heating the sample of **1**, the weight loss started at around 40 ˚C. A narrow plateau with a weight loss of 3.3% appeared at around 70 ˚C and then the weight decreased again. Above 83 ˚C the weight loss reached to 4.3%, which exactly corresponds to the weight of two water molecules per the formula for **1**. This is in good agreement with the elemental analysis for **1**. Very interestingly, on heating the dehydrated sample obtained by heating the sample **1** up to 120 ˚C, a two-step weight loss of 3.2% was observed as shown in Figure 1. This suggests that the dehydrated sample absorbed something after cooling to room temperature. The microanalysis of the cooled dehydrated sample indicated that the composition was $[Fe(\mathbf{L})_2](BF_4)_2 \cdot 1.4H_2O$, whose amount of water is consistent with the proportion of the weight loss of 3.2% from the TG-DTA measurement. We designate this cooled dehydrated sample $[Fe(\mathbf{L})_2](BF_4)_2 \cdot nH_2O$ (n = 1.4) as partly hydrated compound **2** hereafter.

To confirm the structural changes upon dehydration, the powder X-ray diffractions (PXRD) were collected using a RIGAKU SmartLab X-ray diffractometer. The PXRD patterns for **1**, the samples after thermal treatments of **1**, and **3** along with the simulated patterns from the crystal structural data of **1** and **3** are shown in Figure 2. The observed PXRD patterns for the dihydrate compound **1** and anhydrous compound **3** were in good agreement with the

corresponding patterns simulated from the crystal structures of **1** and **3**, respectively. On the other hand, both PXRD patterns for the samples obtained by heating **1** up to 50 and 120 ˚C were completely different from those for **1** and **3** and very similar to each other. This means that the partly hydrated compound **2** belongs to a third crystalline phase. Note that the PXRD pattern for the sample obtained by heating **1** up to 200 ˚C was exactly the same as that for the anhydrous compound **3**. To gain an insight into the thermal crystal structural phase transformation from **2** to **3**, the TG-DTA for **1** was performed up to 200 ˚C (Figure S1). The broad exothermic peak in the DTA curve was observed at around 155 ˚C. This suggests that the crystalline phase of the compound **2** was transformed to that of the anhydrous compound **3** at around 155 ˚C. Hence, the crystal structural phase transformation from the dihydrate compound **1** to anhydrous compound **3** through partly hydrated compound **2** was confirmed.

Magnetic Susceptibility

The temperature variations of magnetic susceptibility for compounds **1**, **2**, and **3** are shown in Figure 3. The $\chi_M T$ value for the anhydrous compound **3** at 300 K was almost zero, suggesting **3** was in the LS state. On heating the sample, the $\chi_M T$ values were gradually increased and reached to 2.85 cm^3 K mol^{-1} at 400 K ($T_{1/2}$ = 351 K). This magnetic behavior is in good agreement with that reported in the literature.[39] The dihydrate compound **1** showed a complete different magnetic behavior. The $\chi_M T$ value for **1** at 300 K was 3.70 cm^3 K mol^{-1}, suggesting **1** was in the HS state. With decreasing temperatures, the $\chi_M T$ values gradually decreased, indicative of the occurrence of an SCO conversion below room temperature. Below 150 K, the $\chi_M T$ value for **1** was almost zero and thus the dihydrate compound **1** exhibited a complete gradual SCO transition ($T_{1/2}$ = 236 K). No apparent thermal hysteresis loop in the

heating and cooling cycle was observed for compounds **1** and **3**. Note that the partly hydrated compound **2** exhibited a very interesting two-step magnetic transition. The higher temperature step was an abrupt transition with a thermal hysteresis of 16 K ($T_{1/2}$(HT) = 202 K), while the lower temperature step was a relatively gradual transition with a thermal hysteresis of 5 K ($T_{1/2}$(LT) = 164 K).

Interestingly, when the magnetic susceptibility for the dihydrate compound **1** was measured using an aluminum capsule with a pinhole, the $\chi_M T$ traces were gradually changed by repeating the cooling and heating scans (Figure S2), leading to an abrupt SCO transition at 194 K with a narrow thermal hysteresis loop of 2 K (Figure 3). The PXRD pattern of the sample exhibiting the one-step abrupt transition corresponded to that of compound **2**. As described above, this change in magnetic behavior seems to arise from the dehydration-associated crystal structural transformation of **1** to **2** in the MPMS chamber. Because of no change of this one-step abrupt transition by further cooling and heating scans, we designate the sample showing the one-step abrupt transition as almost anhydrous compound **2'**, whose exact composition was difficult to determine due to quick absorption of water.

To obtain the thermodynamic parameters from the magnetic susceptibility data, the temperature dependence of $\chi_M T$ for **1**, **2'** and **3** was fitted by the regular-solution model[34] expressed by

$$\ln\left[\frac{1-\gamma_{HS}}{\gamma_{HS}}\right] = \frac{\Delta H + \Gamma(1-2\gamma_{HS})}{RT} - \frac{\Delta S}{R} \qquad (1)$$

where γ_{HS} denotes the HS fraction, ΔH and ΔS denote enthalpy and entropy differences, Γ denotes interaction energy concerning cooperativity, and R is the gas constant. The $\chi_M T$ values

for the pure HS and pure LS states were assumed to be 3.8 and 0 cm^3 K mol^{-1}. The best fit parameters are shown in Table 1. The simulated curves for all compounds reproduce the observed magnetic susceptibility data well (Figure S3). The entropy difference of 125 J K^{-1} mol^{-1} for **1** is much larger than those of 50 to 80 J K^{-1} mol^{-1} for typical SCO Fe^{II} compounds,[3] whereas the entropy difference of 76.3 J K^{-1} mol^{-1} for **2'** is moderate and slightly larger than that of 69.4 J K^{-1} mol^{-1} for **3**. Since the contributions to ΔS from the change in spin multiplicity and intramolecular vibrations should be similar to each other in the solvate compounds, the significant entropy difference between **1** and **2'**/**3** may originate from the water molecules included in the compounds. On the other hand, the interaction energy involved in SCO cooperativity is negligible for **1**, whereas the interaction energy of for **2'** is significant and relatively larger than that for **3**.

Mössbauer Spectroscopy

To confirm the spin and valence states of the Fe ion, the temperature valuable Mössbauer spectra for **1**, **2**, and **3** were recorded (Figure 4). Unfortunately, when we tried to record the Mössbauer spectrum for **2** at 293 K, only the spectrum for **3** at 293 K described below could be obtained and thus it was not successful to record the spectrum for **2**. This suggests the structural transformation from **2** to **3** could be accelerated by a γ-ray irradiation and be completed within a several hours. Figure S4 shows the temperature dependence of Mössbauer spectra for **1** and **3**. The isomer shift (IS) and quadrupole splitting (QS) for **1** and **3** at 10.3 and 293 K are listed in Table 2. Although both **1** and **3** gave only one symmetric quadrupole doublet spectrum at 293 K, the IS values for **1** and **3** were quite different. As compared with the parameters of the $[Ni(dmit)_2]$ compound (Table 2),[38] the spectrum of **3** was ascribed to the Fe^{II} LS state. Except for

broadening the linewidth of a spectrum, the Mössbauer parameters for **3** were unchanged between 10.3 and 293 K. This clearly indicates that the anhydrous compound **3** was in the pure Fe^{II} LS state in the temperature range measured. For the dihydrate compound **1** a doublet spectrum was transformed to a slightly asymmetric one and moreover the IS shifted to the lower velocities at 10.3 K. The IS and QS values for **1** at 10.3 K were quite similar to those of **3**, indicating that **1** was in the Fe^{II} LS state. Consequently, the doublet spectrum with an IS value of 0.8010(6) mm s^{-1} at 293 K can be attributed to the Fe^{II} HS species in **1**. The thermal variation of the Mössbauer parameters from the LS to HS states for **1** was consistent with that from 293 to 350 K for the $[Ni(dmit)_2]$ compound[38] (Table 2). All these observations are in good agreement of the temperature dependence of magnetic susceptibility for **1** and **3**. Hence the dihydrate compound **1** proved to exhibit a complete SCO transition. It should be mentioned that Baker and Goodwin reported that an anhydrous compound showed asymmetric quadrupole doublets with IS = 0.71(4), QS = 1.22(5) mm s^{-1} and IS = 0.47(4), QS = 1.07(5) mm s^{-1} at 77 and 300 K, respectively (Table 2).[39] Although an asymmetric doublet was observed by using a polycrystalline sample of **3**, the symmetric doublet shown in Figure S4 could be obtained by using the same polycrystalline sample grinded. Therefore, the asymmetric spectrum can be originated from the preferred orientation of thin platelets of an anhydrous compound. On the other hand,the reason for the disagreement of the Mössbauer parameters between the present anhydrous compound **3** and Goodwin's anhydrous compound is unclear. We can assume that Goodwin's anhydrous compound might contain a dihydrate compound.

Optical properties

Baker and Goodwin reported that the acetone solution of an anhydrous compound showed a gradual SCO conversion from the HS to LS states with decreasing temperatures from

298 to 193 K.[39] To clarify the LS and HS absorption bands of the [Fe(**L**)$_2$] cation, the temperature variations in UV-vis spectrum for the acetone solution of **3** were recorded in the temperature range of 198−303 K (Figure 4). The absorption spectrum at 303 K revealed that there was a shoulder-like absorption at 460 nm and no other notable absorption in the wavelength range of 550−1100 nm. On lowering temperatures, the absorption maxima of 364 and 467 nm were gradually developed and the isosbestic point appeared at 357 nm. This indicates that the change in UV-vis spectrum originates from the equilibrium between the LS and HS states and the absorption bands at 364 and 467 nm can be attributed to the LS [Fe(**L**)$_2$] cation. Time-dependent density functional theory (TD-DFT) calculations for the optimized LS and HS [Fe(**L**)$_2$] cations (Tables S1−S3) suggest that the absorption at 467 nm is mainly ascribed to the ligand-centered transition band with a small contribution of the ligand-to-metal charge transfer (LMCT) band, whereas that at 364 nm originates mainly from the metal-to-ligand charge transfer (MLCT) band.

To investigate photo responses of the [Fe(**L**)$_2$] compounds, the magnetic susceptibility measurements were performed before and after photo irradiations to each compound. Unfortunately it was difficult to examine the compounds **1** and **2** due to dehydration in the MPMS chamber. On illumination with a YAG laser of 532 nm at 3 K, the magnetization of **3** was increased. This suggests that the photo-induced HS state could be trapped. However, the magnetization was relaxed very rapidly just after the photo irradiation was stopped (Figure S5). The relaxation from the HS to LS states in **3** was completed within 20 minutes even at 3 K. On the other hand, no increase in magnetization was observed by using a diode laser irradiation with either 830 or 1060 nm. These observations are consistent with no absorption band of the LS

[Fe(**L**)$_2$] cation in the wavelength range used. The wavelength dependence on the magnetization for **3** clearly revealed that the change in magnetization arises from a photon process.

In contrast to **3**, the photo-induced HS state of compound **2'** was very stable at 5 K after the photo irradiation with a YAG laser. On heating the photo-irradiated sample of **2'**, the $\chi_M T$ values reached to be 2.65 cm^3 K mol^{-1} at 15 K (Figure 5). The apparent decrease in the $\chi_M T$ started at 60 K and the $\chi_M T$ value was completely relaxed at 76.5 K. Further heating the $\chi_M T$ values were traced to the original $\chi_M T$ values, indicating that the photo effect on the magnetization was completely reversible. Therefore, the significant difference in the relaxation from the photo-induced state between almost anhydrous compound **2'** and anhydrous compound **3** was manifest.

Crystal Structural Analyses for Compounds 1 and 3

To gain an insight into the mechanism of the crystal structural transformation and the SCO behavior variations by thermal and photo effects, the temperature variable X-ray crystal structural analyses for **1** and **3** were performed using a Bruker AXS APEX2 ULTRA system. The crystallographic data for **1** and **3** are listed in Table S4. The coordination bond lengths and the distortion parameters (Σ, Θ) are listed in Table 3. Selected intermolecular distances are listed in Table S5.

The crystal structures for **1** at 180, 220, and 296 K were isostructural and belonged to monoclinic system with *C*2/*c*. The asymmetric unit contained one Fe cation, two BF_4 anions, and two H_2O molecules (Figure 6a). We hereafter designate the ligands including the S1 and S4 atoms as ligand A and B, the water molecules including the O1 and O2 atoms as water molecule

A and B, and the BF_4 anions including the B1 and B2 atoms as anion A and B, respectively. The ligands were coordinated to a central Fe atom as a tridentate ligand and thus two coordinated ligands A and B were arranged in an almost perpendicular manner. The average coordination bond length of **1** at 180 K was 1.996(7) Å, whereas those at 220 and 296 K were 2.054(9) and 2.173(7) Å, respectively, indicating that the dihydrate compound **1** exhibited a gradual SCO conversion. On the other hand, relatively smaller change in Σ and Θ values was observed upon the SCO conversion. This small change in coordination structure may give rise to the smaller variation in QS value of Mössbauer spectrum.

The molecular arrangements for **1** at 180 K are depicted in Figures 6b−6e. Interestingly, there were weak π-stacking interactions and short S···S contacts between the neighboring divalent Fe cations despite strong Coulomb repulsion expected (Figure 6b). The mean π-plane and S···S distances at 180 K were 3.707 and 3.5267(13) Å, respectively (Figure 6c and Table S5). These intermolecular interactions construct a one-dimensional (1D) Fe cation array along the *b* axis (Figure 6b). Anion B and water molecule B were alternately arranged in the direction parallel to the 1D Fe cation array. The distances from the F7 and F5 atoms in anion B to the O2 atom in water molecule B were 2.800(5) and 2.935(5) Å, respectively. Since the sum of van der Waals radii of the oxygen and fluorine atoms is 2.99 Å,[41] the anions B and water molecules B were alternately arranged and formed a 1D hydrogen-bonded molecular array. Furthermore, the distances between the S3 atom in the Fe cation and the F5 atoms in anion B was 3.098(4) Å, which was shorter than the sum of van der Waals radii of the sulfur and fluorine atoms (3.27 Å),[41] and moreover, the C15-S3···F5 angle was 163.73(15) °. This indicates that there were weak chalcogen-bonding-like interactions between the 1D Fe cation and 1D hydrogen-bonded anion-water arrays (Figure 6d). Although two of the 1D Fe cation arrays were bridged by the 1D

alternate anion-water array through chalcogen-bonding-like interactions, no other intermolecular interaction between the 1D Fe cation arrays was observed. With respect to anion A, the intermolecular distances from the O1 atom in water molecule A to the F1 and F4 atoms in anion A were 2.785(4) and 2.839(4) Å at 180 K, respectively. Thus, the anions A formed a hydrogen-bonded dimer through two water molecules A (Figure 6e). The hydrogen-bonded anion dimers were arranged in the direction almost perpendicular to the 1D Fe cation array along the *c* axis. There was no notable short distance between the 1D Fe cation arrays and the hydrogen-bonded anion A dimers. Therefore, the 1D Fe cation array was completely isolated.

As compared with the short contacts at 180 K, all the short contacts involved in π-stacking, sulfur-sulfur, and chalcogen-bonding interactions were lengthened at 296 K. Note that the intermolecular distance between the O2 and F5 atoms was longer than the sum of van der Waals radii, suggesting that the hydrogen-bonding interaction was weakened in the HS state. Therefore, all the intermolecular interactions in the HS state were much weaker than those in the LS state.

The crystal structure for **3** at 253 K belonged to triclinic system with $P\bar{1}$, whereas that at 423 K belonged to tetragonal $I4_1/a$. The asymmetric unit contained one Fe cation and two BF_4 anions at 253 K (Figure 7a), while a quarter of Fe cation and a half of BF_4 anion at 423 K (Figure 7b). The average coordination bond length of **3** at 253 K was 1.980(7) Å, which exactly corresponds to that of **1** at 180 K. The Σ and Θ values for **3** at 253 K were also in good agreement with those of **1** at 180 K (Table 3). Therefore, the anhydrous compound **3** was in the pure LS state at 253 K. On the other hand, the coordination structure of **3** at 423 K corresponded to that of **1** at 296 K, indicative of the occurrence of an SCO conversion from the LS to HS states.

The molecular arrangements for **3** at 253 K are depicted in Figures 7c−7e. There were weak π-stacking interactions and several short S···S contacts between the neighboring Fe cations in **3** (Figure 7c). The mean π-distances between thiazole rings containing the S1 and S2 atoms and containing the S3 and S4 atoms were 3.539 and 3.696 Å, respectively (Table S5). These shorter distances suggest that the intermolecular interactions in **3** are much stronger than those in **1**. These interactions built up a 2D Fe cation network parallel to the *ab* plane (Figure 7d). Anions A were arranged in a 1D manner along the *b* axis in front of the 2D square Fe cation arrangement, while anions B were arranged along the *a* axis behind the 2D layer (Figure 7e). All anions A and B were embedded almost in the center between the 1D Fe cation arrays along the *b* and *a* axes, respectively. Since this Fe cation and BF_4 anion layer was stacked in a front-to-front and back-to-back manner along the *c* axis, the layered structure was constructed in such a manner as anion A layer···Fe cation layer···anion B layer···Fe cation Layer···anion A layer. Note that short intermolecular distances between all the C atoms at the 5-position of a thiazole ring and the corresponding F atoms in BF_4 anions (Table S5) were shorter than the sum of van der Waals radii of the C and F atoms of 3.17 Å.[44] Since their molecular geometries have no characteristic of a directional intermolecular interaction such as a chalcogen-bonding or hydrogen-bonding interaction, these short contacts are considered to result from strong Coulomb interactions between the Fe cation and BF_4 anion. Since the nearest neighboring BF_4 anions can screen the 2D close-packed Fe cation arrays from the Coulomb repulsion between the Fe cations, the 2D π-stacking and sulfur-sulfur interactions between the Fe cations can be enhanced. Therefore, the interplay between the Coulomb, π-stacking, and sulfur-sulfur interactions gave rise to the 3D closed-packed structure in **3**.

The π-stacking and sulfur-sulfur distances between the Fe cations were much lengthened at 423 K, which corresponded to that in **1** at 296 K. Therefore, the intermolecular interactions in the HS state were also much weaker than those in the LS state as in **3**.

Discussion

Possible Mechanism of the Crystal Structure Transformation upon Dehydration

First a possible mechanism of the crystal structural transformation from **1** to **3** through **2** is discussed from the point of view of the structural difference between **1** and **3**. There are two different sites of water molecules in the crystal structure of **1**. Water molecules A were bound in the hydrogen-bonded anion dimer, whereas water molecules B were involved in the hydrogen-bonded 1D anion array. If the water molecules A are removed in the crystal structure, a 1D channel appears along the *b*+*c* direction (Figure 8a). On the other hand, the water molecules B are completely surrounded by the Fe cations and anions B. Therefore, the release of water molecules A from the 1D channel can trigger the present dehydration process in **1**. Subsequently, anions A can move into the 1D channel given by the release of water molecule A.

Since Coulomb interactions are considered to be much stronger than other intermolecular interactions, we should consider Coulomb interactions between the Fe cation and anions A to suppose a possible motion of the Fe cations. The Fe···B distances between the Fe cation and its nearest neighboring anions A in **1** are listed in Table S6. It should be noted that the Fe···B distance of 5.377(7) Å between the Fe cation and anion A with a symmetry operation of (x, 1-y, 0.5+z) in **1** was significantly shorter than the other Fe···B distances, whose positions are indicated by yellow green double-headed arrows in Figures 8a and 8c. This strong attractive

Coulomb interaction between the Fe cation and anion A implies that the motion of anion A can accompany the motion of the Fe cation.

The neighboring Fe cations along either the *a* or *b* axis in the anhydrous compound **3** are related to a translation operation and thus all the π-ligand planes participating in the π-stacking interactions in each direction are parallel to each other (Figures 8b and 8d). On the other hand, the symmetry relationships between the neighboring Fe cations along the *c* axis and *a*+*c* directions in **1** are glide plane and inversion center operations, respectively. Therefore, the π-ligand planes along the *c* axis are not parallel to each other (Figure 8c), whereas those along the *a*+*c* direction are almost parallel to each other. If a 2D π-stacking Fe cation array in **3** is constructed from 1D π-stacking Fe cation arrays along the *a*+*c* direction in **1**, the molecular rotation angles of the Fe cations in one 1D array and its nearest neighboring 1D array are 0 ° and 180 °, respectively. These alternate rotation motions of the Fe cations are quite unreasonable. If a 2D π-stacking structure in **3** is formed from the 1D π-stacking Fe cation arrays along the *c* axis in **1** (Figure 8c), the original π-stacking interactions between the ligands A in the 1D Fe cation array must disappear and a new π-stacking interaction between the ligands B must be constructed. Although these structural changes seem to be large, the Fe cations in one 1D array and its nearest neighboring 1D array rotate with a similar angle of about 60 ° as if the gears engage (see the difference between Figures 8c and 8d). Note that this rotation motion of the Fe cation may occur along the direction parallel to the above mentioned shortest Fe···B distance between the Fe cation and anion A (Figure 8c). Therefore, we can assume that the motion of the anion A may be followed by the gear-like rotation of the Fe cations.

Figures 8a and 8c summarize the possible motions of each molecule by round arrows in **1** at 296 K. After the release of water molecule A, the anions A can move into the 1D channel and then the Fe cations may rotate in the above mentioned manner. The rotations of the Fe cation may induce the reconstruction of the π-stacking interaction, which may accompany the rotation of the 1D Fe cation array in a counter-clockwise manner shown in Figure 8a. These motions can produce a space around water molecules B which were surrounded by the Fe cations and anions B, promoting the release of water molecules B. Since the anion B is originally arranged along the *b* axis in **1**, the anion B arrays are almost perpendicular to the anion A arrays separated by the 2D Fe cation layer. The assumed crystal structure exactly corresponds to the crystal structure of the anhydrous compound **3** (Figures 8b and 8d).

In order to gain an insight of the crystal structure of **2**, we attempted to analyze the crystal structure of **2** from the PXRD profile. Unfortunately, the PXRD profile measured was gradually changed into that of anhydrous compound **3**, indicating the crystal structure transformation might be induced by X-ray irradiation. Although the crystal structural determination of **2** was not successful, the cell parameters for **2** can be estimated by the diffractogram as follows (Figure S6): monoclinic $P2_1/c$, a = 20.900(2), b = 8.9765(10), c = 19.254(2) Å, α = 90, β = 113.7807(17), γ = 90 °, V = 3305.5(6) Å^3, R_{wp} = 0.0313. The cell volume for **2** is larger than that for **3** at 253 K, while is smaller than half of that for **1** at 296 K. Thus, the order of the volumes per formula unit is **1** > **2** > **3**. These differences in volume correspond to the amount of hydrate water molecules. On the other hand, the absorption and desorption of water molecules in compound **2** suggests the crystal structure of **2'** contains pores which are retained even by complete dehydration. Therefore, we can propose that compound **2'** may have a non-close-packed structure.

What is the driving force for this structural transformation? Twelve short Fe···B distances are varied from 5.377(7) to 10.998(7) Å for **1** at 296 K, while from 6.845(4) to 7.799(5) for **3** at 253 K (Table S6). With respect to Coulomb interaction contribution, the lattice enthalpy in ionic solids is known to be in inverse proportion to the nearest neighboring distances between cation and anion. In the present case, the sum of the reciprocals of twelve Fe···B distances in **1** is 1.580 $Å^{-1}$, whereas that in **3** is 1.627 $Å^{-1}$. Hence the lattice enthalpy for **1** should be smaller than that for **3**. Moreover, the above mentioned comparison between the volumes per formula unit strongly suggests that the order of the lattice enthalpies seems to be **1** < **2** < **3**. Therefore, the present crystal transformation would be driven by Coulomb interactions between the Fe cation and BF_4 anion. Since similar desolvation-induced crystal structure transformation driven by Coulomb energy gain was reported in a charged SCO complex,[42] Coulomb interactions between cation and anion would play a key role in crystal structural phase transitions in ionic molecular solids.

Relationship between the crystal structures and cooperativity in SCO transition

Next we discuss the relationship between the thermodynamic parameters and crystal structures from a point of view of intermolecular interactions. The difference in interaction energy is considered to result from the contribution of intermolecular interactions. As compared with the crystal structures between **1** and **3**, the Fe cations in **1** form a 1D intermolecular array by weak π-stacking, sulfur-sulfur, chalcogen-bonding-like, and hydrogen-bonding interactions, whereas those in **3** gives a 2D intermolecular network by stronger π-stacking and sulfur-sulfur interactions. Since the Coulomb interaction is known to no contribution to the interaction energy

in SCO cooperativity,[42] the π-stacking and sulfur-sulfur interactions and their dimensionality would play a crucial role in the interaction energy in **3**.

On the other hand, the gradual SCO conversion in **3** is quite different from the abrupt SCO transition in **2'** despite the interaction energies comparable to each other. It should be noted that the enthalpy difference in **2'** was much less than that in **3** (Table 1). The enthalpy difference between the LS and HS states originates from the difference in the sum of the energies from the molecular components and crystal lattice for each spin state. Since the energies of the molecular components between polymorphs like almost anhydrous compound **2'** and anhydrous compound **3** should be similar to each other, the main contribution to the enthalpy difference should arise from the difference in lattice enthalpy between the HS and LS states. The Kapustinskii equation[43] is well-known to estimate the lattice enthalpy from Coulomb interactions in ionic crystals by using the mean cation-anion distance. The substitution of the mean cation-anion distances of 7.39 and 7.64 Å at 253 and 423 K in the Kapustinskii equation gives the lattice enthalpies of 936 and 907 kJ mol^{-1}, respectively. Thus, the lattice enthalpy difference of 29 kJ mol^{-1} in **3** surprisingly agrees with the enthalpy difference of 26.9 kJ mol^{-1} simulated from the magnetic susceptibility measurement. Since the largest energy of π-stacking interactions of a thiophene dimer similar to **3** is calculated to be −7.15 kJ mol^{-1}, [44] the lattice enthalpy difference is suggested to arise mainly from Coulomb interactions in the present compounds.

Our present finding suggests the enthalpy difference between the HS and LS states arising from Coulomb interactions may govern the SCO behavior in the case of ionic SCO polymorphs. This idea can also be applied to the account for the large difference in relaxation temperature from the photo-induced HS state between **2'** and **3**. The linear relationship between

the relaxation temperature from the light-induced excited spin-state trapping (LIESST) state (T_{LIESST}) and the SCO transition temperature ($T_{1/2}$) was proposed.[44] This proposal is based on the assumption that the SCO derivatives or analogues have a similar entropy difference in SCO transition and thus the enthalpy difference can govern the SCO transition temperature. The application of this linear relationship to **2'** leads to an equation of $T_{LIESST} = 130 - 0.3T_{1/2}$. The substitution of the SCO transition temperature of **3** in this equation gives $T_{LIESST} = 25$ K. Therefore, the trend of the relaxation temperatures can be interpreted by the large enthalpy differences between **2'** and **3**. Hence the contribution of Coulomb interactions to the enthalpy difference in SCO transition may play a crucial role in the SCO behavior of ionic SCO compounds.

Conclusion

We have carried out the characterization of a series of $[Fe^{II}(\mathbf{L})_2]$ compounds, dihydrate compound **1**, partly hydrated compounds **2** and **2'**, and anhydrous compound **3**. The crystal structural phase transformation from **1** to **3** through **2** and **2'** upon dehydration was evidenced by the PXRD and magnetic susceptibility experiments. As compared with the crystal structures for **1** and **3**, this crystal transformation seems to be driven by relatively strong Coulomb interactions between the Fe cation and BF_4 anion. Furthermore, the SCO behaviors in a series of compounds may be governed by the Coulomb interaction which mainly contributes to the enthalpy difference in SCO transition. To the best our knowledge, this is the first evidence for the contribution of Coulomb interactions to SCO behaviors and crystal structural phase transitions. Recently the desolvation-induced phase transformations in the charged SCO compounds were reported.[46,47] Our finding can shed a light on elucidation of the mechanism of SCO behavior variations and phase transformations in charged SCO compounds.

So far the introduction of intermolecular interactions between SCO molecules has been considered to be important to achieve the cooperativity in SCO transition. However, the present study reveals that the introduction of strong intermolecular interactions supported by Coulomb interactions lead to a large enthalpy difference between the LS and HS states, which will suppress the cooperative SCO transition and give rise to a very fast relaxation from the photo-induced metastable HS state in **3**. Therefore, the contribution of Coulomb interactions must be taken into account to control the cooperativity in charged SCO compounds.

Table 1. Thermodynamic parameters of SCO transitions.

Compounds	ΔH / kJ mol^{-1}	Γ / kJ mol^{-1}	ΔS / J K^{-1} mol^{-1}
1	28.7	0	125
2'	17.1	0.99	76.3
3	26.9	0.61	69.4

Table 2. Temperature variations of Mössbauer parameters for **1** and **3**.

Compounds	Temperature / K	IS[a] / mm s^{-1}	QS[b] / mm s^{-1}	LW[c] / mm s^{-1}
1	293	0.8010(6)	0.8940(11)	0.2880(15)
	10.3	0.3510(11)	1.111(2)	0.586(3)
3	293	0.2750(2)	1.2120(4)	0.2790(6)
	10.3	0.307(3)	1.218(5)	1.236(8)
$[Fe(\mathbf{L})_2][Ni(dmit)_2]_2$[d]	350	0.557(2)	1.166(4)	-
	293	0.2806(4)	1.1123(8)	-
	8.6	0.3189(15)	1.056(3)	-

$[Fe(\mathbf{L})_2](BF_4)_2$[e]	300	0.47(4)	1.07(5)	-
	77	0.71(4)	1.22(5)	-

[a]Isomer shift. [b]Quadrupole splitting. [c]Linewidth. [d]Reference 38. [e]Reference 39. The parameters were calibrated by sodium nitroprusside.

Table 3. Selected bond lengths (Å) and angles (°) of **1** and **3**.

Compound	**1**			**3**	
Temperature / K	180	220	296	253	423
Fe1-N1	2.034(3)	2.099(4)	2.209(3)	2.030(3)	2.166(3)
Fe1-N2	1.923(3)	1.988(4)	2.112(3)	1.908(3)	2.074(5)
Fe1-N3	2.023(3)	2.075(4)	2.204(3)	2.013(3)	2.166(3)
Fe1-N4	2.029(3)	2.079(4)	2.193(3)	2.014(3)	2.166(3)
Fe1-N5	1.928(3)	1.989(4)	2.105(3)	1.911(3)	2.074(5)
Fe1-N6	2.036(2)	2.096(3)	2.219(3)	2.008(3)	2.166(3)
Σ^a	82.9(4)	99.4(5)	129.5(4)	77.9(4)	123.1(3)
Θ^b	142.4(4)	166.0(6)	208.7(5)	137.1(5)	199.7(5)

[a] The sum of the deviations of the bite angles from 90 °. [b] The sum of the absolute differences of all the angles of triangle surfaces of a coordination octahedron from 60 °.

Chart 1. Molecular structures of $[Fe^{II}(\mathbf{L})_2](BF_4)_2$ compounds.

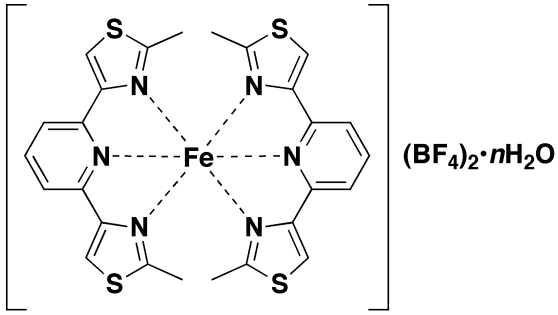

1 : $n = 2$
2 : $n = 1.4$
2' : $n \sim 0$
3 : $n = 0$

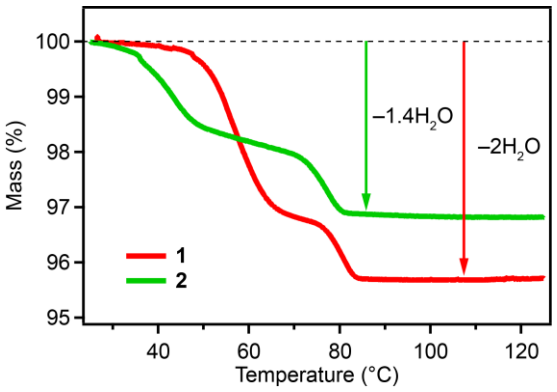

Figure 1. TG curves for **1** and **2**.

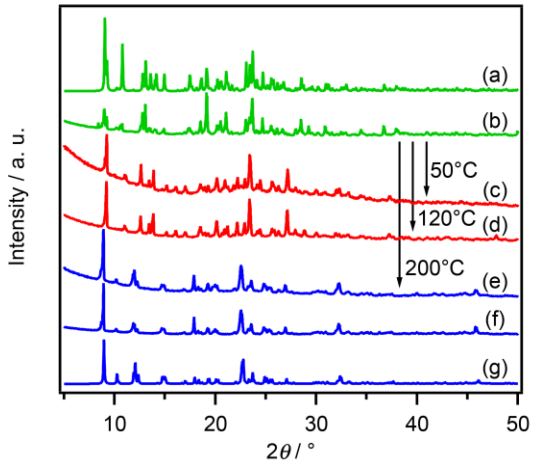

Figure 2. Powder X-ray diffractograms at room temperature. The simulated profile from the crystal structure of **1** (a). The observed profiles for **1** (b), for **1** after heated to 50 ˚C (c), for **1** after heated to 120 ˚C (d), for **1** after heated to 200 ˚C (e), and for **3** (f). The simulated profile from the crystal structure of **3** (g).

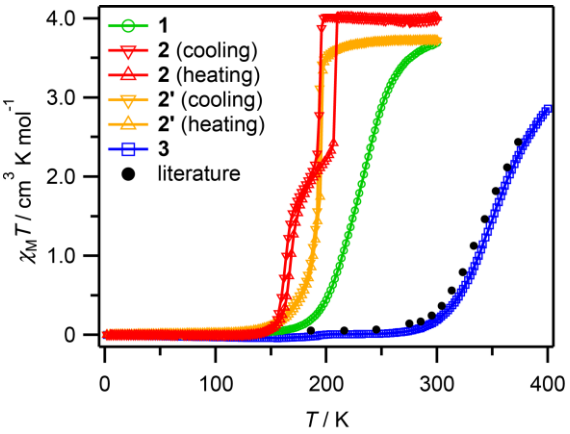

Figure 3. Temperature variations of the $\chi_M T$ products at a scan rate of 2 K min^{-1} for **1**, **2**, and **3** and at a scan rate of 1 K min^{-1} for **2'**. Black circles indicate the calculated $\chi_M T$ values for an anhydrous compound reported by the previous literature [39].

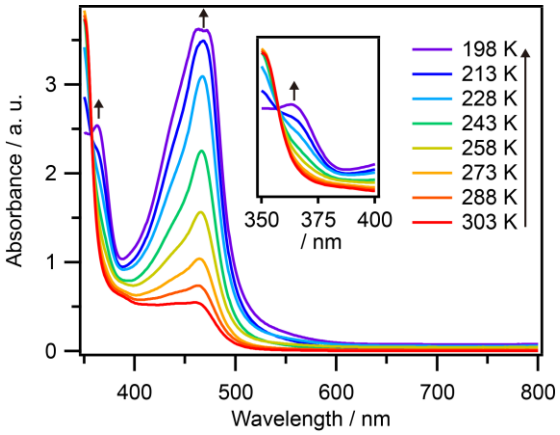

Figure 4. Temperature dependence of UV-vis spectra for an acetone solution of **3**.

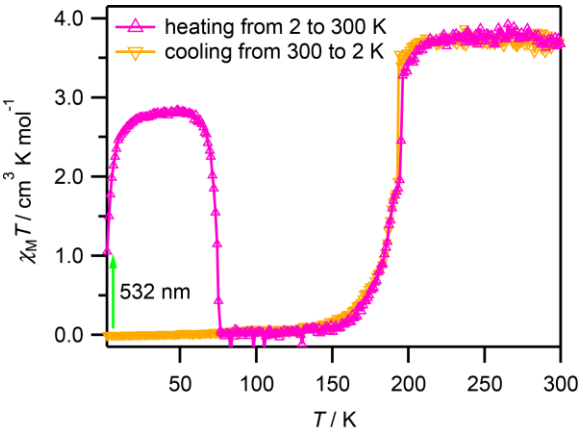

Figure 5. Temperature variations of the $\chi_M T$ products for **2'** at a scan rate of 1 K min^{-1} before and after photo irradiation with 532 nm.

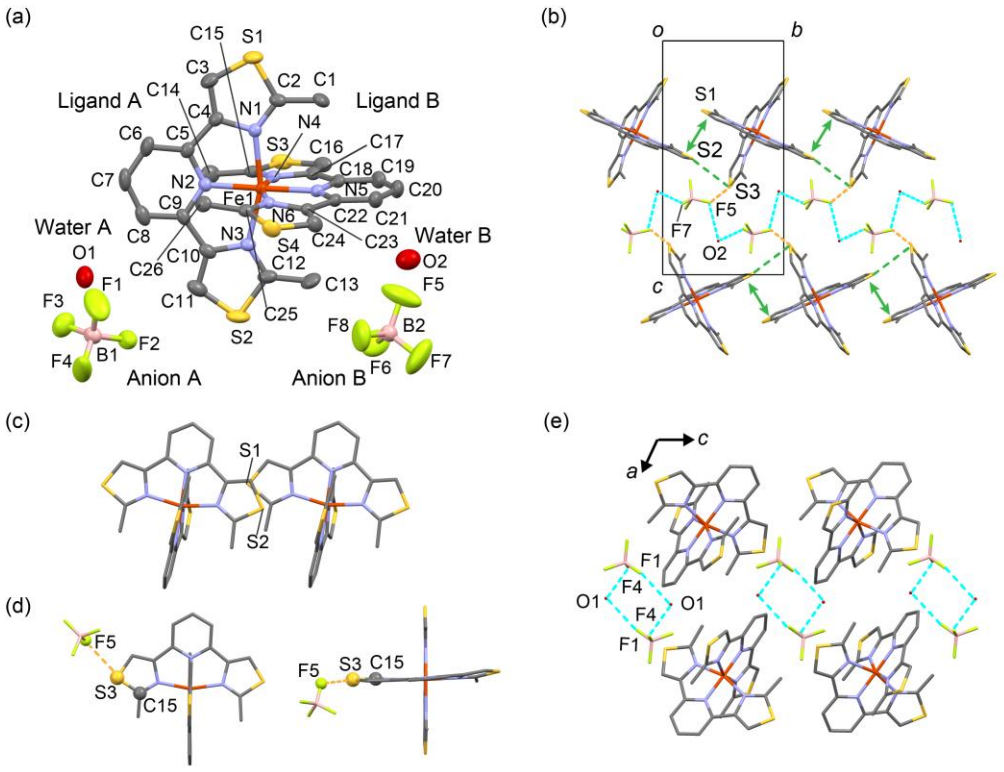

Figure 6. Crystal structure of **1** at 180 K. (a) ORTEP diagrams of 50% probability with atomic numbering. Hydrogen atoms are omitted for clarity. (b) 1D molecular arrays of the Fe cations, anions B, and water molecules B viewed along the *a* axis. Green double-headed arrows indicate the positions of π-stacking interactions. Green, cyan, and orange broken lines represent S···S, O···F, and S···F short distances, respectively. (c) Top view of the π-overlap between the Fe cations. (d) Molecular arrangement involving in the chalcogen-bonding-like interaction. (e) Molecular arrays from the Fe cations and anion A dimers. Cyan broken lines indicate O···F short distances.

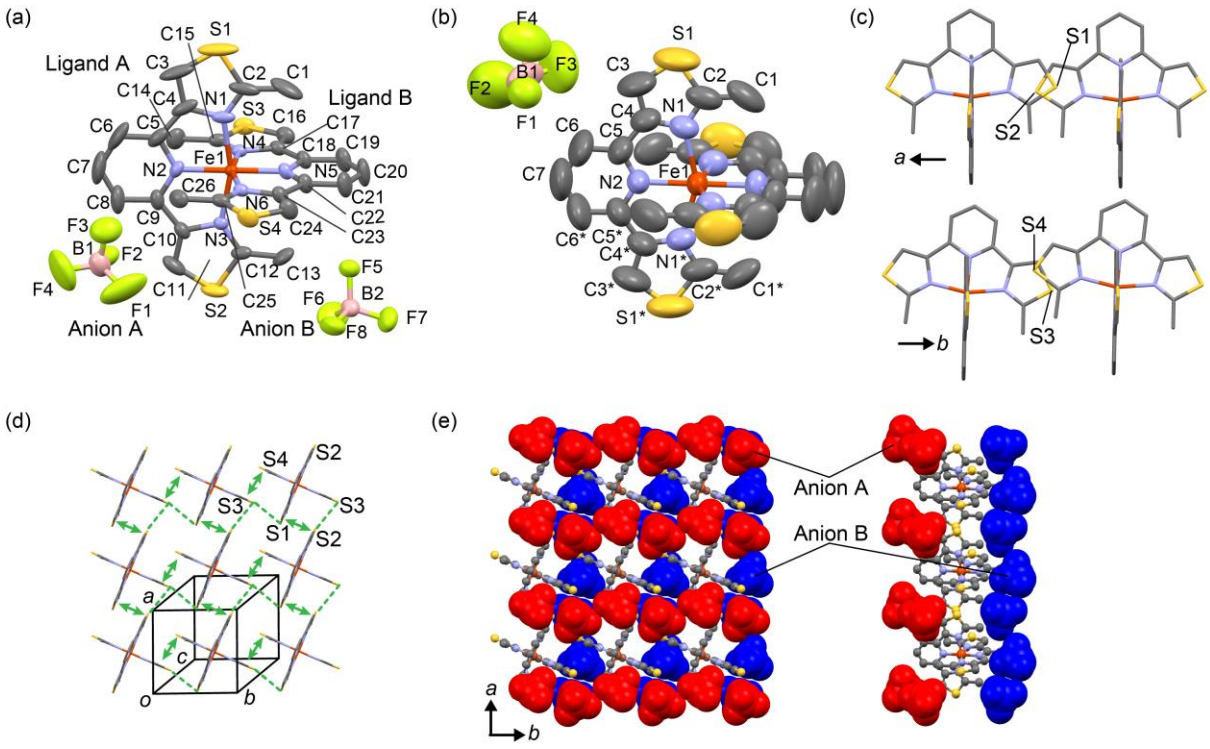

Figure 7. Crystal structures of **3**. ORTEP diagrams of 50% probability with atomic numbering at 253 K (a) and 423 K (b). Hydrogen atoms are omitted for clarity. The atomic numbers with an asterisk indicate the atoms generated by a symmetry operation.(c) Top view of the π-overlaps between ligands at 253 K. (d) 2D molecular arrangement of the Fe cations at 253 K. Green double-headed arrows and broken lines indicate the π-stacking interactions and short S···S contacts less than 3.7 A, respectively. (e) Packing diagram for the BF_4 anion layers and Fe complex cation layer at 253 K. Red and blue anions are anion A and anion B, respectively.

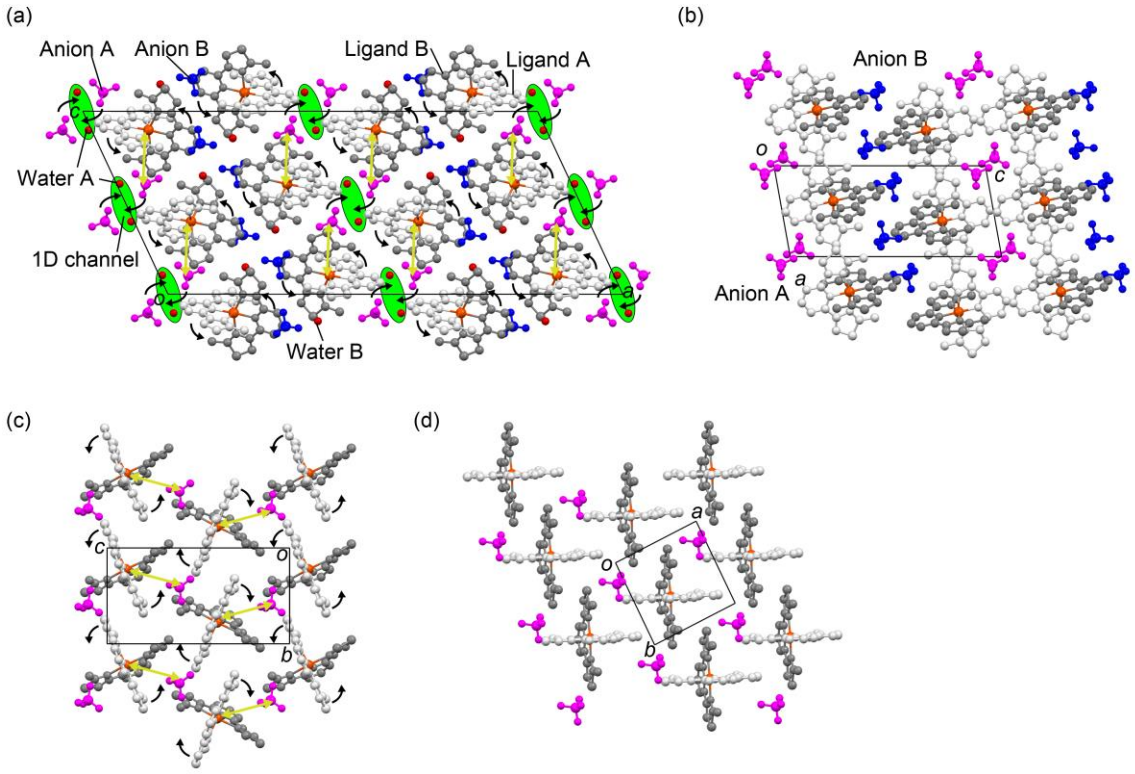

Figure 8. (a) Crystal structure for **1** at 296 K viewed along the *b* axis. (b) Crystal structure for **3** at 253 K viewed along the *b* axis. Fe cation arrays with the nearest neighboring anions A parallel to the *bc* plane in **1** at 296 K (c) and to *ab* plane in **3** at 253 K (d). Yellow green double-headed arrows indicate the nearest cation···anion distances. Light grey and dark grey ligands are ligands A and B, respectively. Magenta and blue anions are anions A and B, respectively. Green filled ovals indicate 1D channels given by the release of water molecules A. Black round arrows mean possible motions of the Fe cation and BF_4 anion involved in crystal structural transformation.

ASSOCIATED CONTENT

Supporting Information.

The optimized HS and LS Fe cation coordinates, the calculated excitation wavelengths, oscillator strengths, and the assignments, the crystallographic data, the intermolecular distances, DTA curve, thermal dependent $\chi_M T$ products with fitting curves, the temperature dependence of Mössbauer spectra, time-dependent $\chi_M T$ products after photo irradiation, powder X-ray diffraction profile of **2**. This material is available free of charge via the Internet at http://pubs.acs.org.

AUTHOR INFORMATION

Corresponding Author

*E-mail: ktaka@crystal.kobe-u.ac.jp

ACKNOWLEDGMENT

This work was partially supported by a Grant-in-Aid for Scientific Research (C) (No. 25410068) from the Ministry of Education, Culture, Sports, Science, and Technology of Japan. A part of this work was conducted at Advanced Characterization Nanotechnology Platform of the University of Tokyo, supported by "Nanotechnology Platform" of the Ministry of Education, Culture, Sports, Science and Technology (MEXT), Japan.

REFERENCES

(1) Gütlich, P.; Goodwin, H. A. Eds. *Spin Crossover in Transition Metal Compounds I-III*, Springer-Verlag, Berlin Heidelberg, Germany, 2004.

(2) Halcrow, M. A. Ed. *Spin-Crossover Materials*; John Wiley & Sons, Ltd.: Oxford, United Kingdom, 2013.

(3) Gütlich, P.; Gaspar, A. B.; Garcia, Y. Spin state switching in iron coordination compounds. *Beilstein J. Org. Chem.* **2013**, *9*, 342–391.

(4) Bousseksou, A.; Molnár, G.; Salmon, L.; Nicolazzi, W. Molecular spin crossover phenomenon: recent achievements and prospects. *Chem. Soc. Rev.* **2011**, *40*, 3313−3335.

(5) Létard, J.-F.; Guionneau, P.; Codjovi, E.; Lavastre, O.; Bravic, G.; Chasseau, D.; Kahn, O. Wide thermal hysteresis for the mononuclear spin-crossover compound *cis*-Bis(thiocyanato)bis[*N*-(2'-pyridylmethylene)-4-(phenylethynyl)anilino]iron(II). *J. Am. Chem. Soc.* **1997**, *119*, 10861–10862.

(6) Zhong, Z. J.; Tao, J.-Q.; Yu, Z.; Dun, C.-Y.; Liu, Y.-J.; You, X.-Z. A stacking spin-crossover iron(II) compound with a large hysteresis. *J. Chem. Soc., Dalton Trans.* **1998**, 327–328.

(7) Hayami, S.; Gu, Z.-Z.; Yoshiki, H.; Fujishima, A.; Sato, O. Iron(III) spin-crossover compounds with a wide apparent thermal hysteresis around room temperature. *J. Am. Chem. Soc.* **2001**, *123*, 11644–11650.

(8) Takahashi, K.; Cui, H.-B.; Kobayashi, H.; Einaga, Y. Sato, O. The light-induced excited spin state trapping effect on $Ni(dmit)_2$ salt with an Fe(III) spin-crossover cation: $[Fe(qsal)_2][Ni(dmit)_2]\cdot 2CH_3CN$. *Chem. Lett.* **2005**, *34*, 1240−1241.

(9) Takahashi, K.; Cui, H.-B.; Okano, Y.; Kobayashi, H.; Einaga, Y.; Sato, O. Electrical conductivity modulation coupled to a high-spin−low-spin conversion in the molecular system $[Fe^{III}(qsal)_2][Ni(dmit)_2]_3\cdot CH_3CN\cdot H_2O$. *Inorg. Chem.* **2006**, *45*, 5739−5741.

(10) Kuroda-sawa, T.; Yu, Z.; Senzaki, Y.; Sugimoto, K.; Maekawa, M.; Munakata, M.; Hayami, S.; Maeda, Y. Abrupt spin transitions and LIESST effects observed in Fe^{II} spin-crossover complexes with extended π-conjugated Schiff-base ligands having N_4O_2 donor sets. *Chem. Lett.* **2008**, *37*, 1216−1217.

(11) Takahashi, K.; Mori, H.; Kobayashi, H.; Sato, O. Mechanism of reversible spin transition with a thermal hysteresis loop in $[Fe^{III}(qsal)_2][Ni(dmise)_2]\cdot 2CH_3CN$: Selenium analogue of the precursor of an Fe(III) spin-crossover molecular conducting system. *Polyhedron* **2009**, *28*, 1776−1781.

(12) Phonsri, W.; Macedo, D. S.; Vignesh, K. R.; Rajaraman, G.; Davies, C. G.; Jameson, G. N. L.; Moubaraki, B.; Ward, J. S.; Kruger, P. E.; Chastanet, G.; Murray, K. S. Halogen substitution effects on N_2O Schiff base ligands in unprecedented abrupt Fe^{II} spin crossover complexes. *Chem. Eur. J.* **2017**, *23*, 7052–7065.

(13) Murata, S.; Takahashi, K.; Mochida, T.; Sakurai, T.; Ohta, H.; Yamamoto, T.; Einaga, Y. Cooperative spin-crossover transition from three-dimensional purely π-stacking interactions in a

neutral heteroleptic azobisphenolate Fe^{III} complex with a N_3O_3 coordination sphere. *Dalton Trans.* **2017**, *46*, 5786−5789.

(14) Kröber, J.; Codjovi, E.; Kahn, O.; Grolière, F.; Jay, C. A spin transition system with a thermal hysteresis at room temperature. *J. Am. Chem. Soc.* **1993**, *115*, 9810–9811.

(15) Kitazawa, T.; Gomi, Y.; Takahashi, M.; Takeda, M.; Enomoto, M.; Miyazaki, A.; Enoki, T. Spin-crossover behaviour of the coordination polymer $Fe^{II}(C_5H_5N)_2Ni^{II}(CN)_4$. *J. Mater. Chem.* **1996**, *6*, 119−121.

(16) Niel, V.; Martinez-Agudo, J. M.; Muñoz, M. C.; Gaspar, A. B.; Real, J. A. Cooperative spin crossover behavior in cyanide-bridged Fe(II)-M(II) bimetallic 3D Hofmann-like networks (M = Ni, Pd, and Pt). *Inorg. Chem.* **2001**, *40*, 3838−3839.

(17) Halder, G. J.; Kepert, C. J.; Moubaraki, B.; Murray, K. S., Cashion, J. D. Guest-dependent spin crossover in a nanoporous molecular framework material. *Science* **2002**, *298*, 1762−1765.

(18) Niel, V.; Thompson, A. L.; Goeta, A. E.; Enachescu, C.; Hauser, A.; Galet, A.; Muñoz, M. C.; Real, J. A. Thermal- and photoinduced spin-state switching in an unprecedented three-dimensional bimetallic coordination polymer. *Chem. Eur. J.* **2005**, *11*, 2047–2060.

(19) Ohba, M.; Yoneda, K.; Agustí, G.; Munoz, M. C.; Gaspar, A. B.; Real, J. A.; Yamasaki, M.; Ando, H.; Nakao, Y.; Sakaki, S.; Kitagawa, S. Bidirectional chemo-switching of spin state in a microporous framework. *Angew. Chem. Int. Ed.* **2009**, *48*, 4767−4771.

(20) Ohkoshi, S.; Imoto, K.; Tsunobuchi, Y.; Takano, S.; Tokoro, H. Light-induced spin-crossover magnet. *Nat. Chem.* **2011**, *3*, 564−569.

(21) Clements, J. E.; Price, J. R.; Neville, S. M.; Kepert, C. J. Hysteretic four-step spin crossover within a three-dimensional porous Hofmann-like material. *Angew. Chem. Int. Ed.* **2016**, *55*, 15105−15109.

(22) Murphy, M. J.; Zenere, K. A.; Ragon, F.; Southon, P. D.; Kepert, C. J.; Neville, S. M. Guest programmable multistep spin crossover in a porous 2-D Hofmann-type material. *J. Am. Chem. Soc.* **2017**, *139*, 1330–1335.

(23) Chernyshov, D.; Hostettler, M.; Törnroos, K. W.; Bürgi, H.-B. Ordering phenomena and phase transitions in a spin-crossover compound—Uncovering the nature of the intermediate phase of $[Fe(2\text{-pic})_3]Cl_2 \cdot EtOH$. *Angew. Chem. Int. Ed.* **2003**, *42*, 3825−3830.

(24) Weber, B.; Bauer, W.; Obel, J. An iron(II) spin-crossover complex with a 70 K wide thermal hysteresis loop. *Angew. Chem. Int. Ed.* **2008**, *47*, 10098−10101.

(25) Fujinami, T.; Koike, M.; Matsumoto, N.; Sunatsuki, Y.; Okazawa, A.; Kojima, N. Abrupt spin transition with thermal hysteresis of iron(III) complex $[Fe^{III}(Him)_2(hapen)]AsF_6$ (Him = Imidazole, H_2hapen = *N*,*N*'-Bis(2-hydroxyacetophenylidene)ethylenediamine). *Inorg. Chem.* **2014**, *53*, 2254−2259.

(26) Nemec, I.; Herchel, R.; Trávniček, Z. The relationship between the strength of hydrogen bonding and spin crossover behaviour in a series of iron(III) Schiff base complexes. *Dalton Trans.* **2015**, *44*, 4474−4484.

(27) Hagiwara, H.; Okada, S. A polymorphism-dependent $T_{1/2}$ shift of 100 K in a hysteretic spin-crossover complex related to differences in intermolecular weak CH···X hydrogen bonds (X = S vs. S and N). *Chem. Commun.* **2016**, *52*, 815–818.

(28) Fukuroi, K.; Takahashi, K.; Mochida, T.; Sakurai, T.; Ohta, H.; Yamamoto, T.; Einaga, Y.; Mori, H. Synergistic spin transition between spin crossover and spin-Peierls-like singlet formation in the halogen-bonded molecular hybrid system: $[Fe(Iqsal)_2][Ni(dmit)_2]\cdot CH_3CN\cdot H_2O$. *Angew. Chem. Int. Ed.* **2014**, *53*, 1983−1986.

(29) Nassirinia, N.; Amani, S.; Teat, T. J.; Roubeau, O.; Gamez, P. Enhancement of spin-crossover cooperativity mediated by lone pair‑π interactions and halogen bonding. *Chem. Commun.* **2014**, *50*, 1003−1005.

(30) Takahashi, K.; Kawakami, T.; Gu, Z.-Z.; Einaga, Y.; Fujishima, A.; Sato, O. An abrupt spin transition based on short S···S contacts in a novel Fe(II) complex whose ligand contains a 1,3-dithiole ring. *Chem. Commun.* **2003**, 2374−2375.

(31) Tuchagues, J. P.; Bousseksou, A.; Molnár, G.; McGarvey, J. J.; Varret, F. The Role of Molecular Vibrations in the Spin Crossover Phenomenon. In *Spin Crossover in Transition Metal Compounds III*, Gütlich, P., Goodwin, H. A. Eds.; Springer-Verlag, Berlin Heidelberg, Germany, 2004, pp. 85–103.

(32) Spiering, H. Elastic Interaction in Spin Crossover Compounds. In *Spin Crossover in Transition Metal Compounds III*, Gütlich, P., Goodwin, H. A. Eds.; Springer-Verlag, Berlin Heidelberg, Germany, 2004, pp. 171–195.

(33) Kahn, O. In *Molecular Magnetism*; Wiley-VCH, New York, USA, 1993, Chapter 4, pp. 53–86.

(34) Slichter, C. P.; Drickamer, H. G. Pressure-induced electronic changes in compounds of iron. *J. Chem. Phys.* **1972**, *56*, 2142-2160.

(35) Sorai, M.; Seki, S. Phonon coupled cooperative low-spin $^1A_1$ ™ high-spin $^5T_2$ transition in $[Fe(phen)_2(NCS)_2]$ and $[Fe(phen)_2(NCSe)_2]$ crystals. *J. Phys. Chem. Solids* **1974**, *35*, 555-570.

(36) Purcell, K. F.; Edwards, M. P. Cooperativity in thermally induced intersystem crossing in solids: $Fe(phen)_2(NCR)_2$, R = BH_3, BPh_3, S, Se. *Inorg. Chem.* **1984**, *23*, 2620-2635.

(37) Martin, J.-P.; Zarembowitch, J.; Bousseksou, A.; Dworkin, A.; Haasnoot, J. G.; Varret, F. Solid state effects on spin transitions: Magnetic, calorimetric, and Mössbauer-effect properties of $[Fe_xCo_{1-x}(4,4'\text{-bis-}1,2,4\text{-triazole})_2(NCS)_2]\cdot H_2O$ mixed-crystal compounds. *Inorg. Chem.* **1994**, *33*, 6325–6333.

(38) Okai, M.; Takahashi, K.; Sakurai, T.; Ohta, H.; Yamamoto, T.; Einaga, Y. Novel Fe(II) spin crossover complexes involving a chalcogen-bond and π-stacking interactions with a paramagnetic and nonmagnetic $M(dmit)_2$ anion (M = Ni, Au; dmit = 4,5-dithiolato-1,3-dithiole-2-thione). *J. Mater. Chem. C* **2015**, *3*, 7858−7864.

(39) Baker, A.T.; Goodwin, H. A. Iron(II) and nickel(II) complexes of 2,6-di(thiazol-4-yl)pyridine and related ligands: Magnetic, spectral and structural studies. *Aust. J. Chem.* **1986**, *39*, 209−220.

(40) König, E. Magnetische suszeptililitäten: Einleitung in *Landolt-Börnstein Neue Serie II*, König, E. Ed., Springer-Verlag, Berlin Heidelberg, Germany, 1981, pp. 1-16–18.

(41) Bondi, A. van der Waals Volumes and Radii. *J. Phys. Chem.* **1964**, *68*, 441−451.

(42) Murata, S.; Takahashi, K.; Sakurai, T.; Ohta, H.; Yamamoto, T.; Einaga, Y.; Shiota, Y.; Yoshizawa, K. The role of Coulomb interactions for spin crossover behaviors and crystal

structural transformation in novel anionic Fe(III) complexes from a π-extended ONO ligand. *Crystals* **2016**, *6*, 49 (16 pages).

(43) Kapustinskii, A. F. Lattice energy of ionic crystals. *Q. Rev. Chem. Soc.* **1956**, *10*, 283–294.

(44) Tsuzuki, S; Honda, K.; Azumi, R. Model Chemistry Calculations of Thiophene Dimer Interactions: Origin of π-Stacking. *J. Am. Chem. Soc.* **2002**, *124*, 12200–12209.

(45) Létard, J.-F.; Guionneau, P.; Nguyen, O.; Costa, J. S.; Marcén, S.; Chastanet, G.; Marchivie, M.; Goux-Capes, L. A guideline to the design of molecular-based materials with long-lived photomagnetic lifetimes. *Chem. Eur. J.* **2005**, *11*, 4582–4589.

(46) Roberts, T. D.; Tuna, F.; Malkin, T. L.; Kilner, C. A.; Halcrow, M. A. An iron(II) complex exhibiting five anhydrous phases, two of which interconvert by spin-crossover with wide hysteresis. *Chem. Sci.* **2012**, *3*, 349–354.

(47) Bushuev, M. B.; Pishchur, D. P.; Logvinenko, V. A.; Gatilov, Y. V.; Korolkov, I. V.; Shundrina, I. K.; Nikolaenkova, E. B.; Krivopalov, V. P. A mononuclear iron(II) complex: cooperativity, kinetics and activation energy of the solvent-dependent spin transition. *Dalton Trans.* **2016**, *45*, 107–120.

Insert Table of Contents Graphic and Synopsis Here

The structural and physical characterization of charged Fe^{II} complexes, dihydrate **1**, partly hydrated compounds **2** and **2'**, and anhydrous compound **3**, revealed that the occurrence of two-step crystal structural transformation from the dihydrate to anhydrous compound upon dehydration accompanied the significant change in their spin crossover behaviors, which can be interpreted by the lattice energies arising from Coulomb interactions between the Fe cation and counter anion in typical ionic crystals.